Numerical Investigation of the Flow Field in HP Turbine Stage

Francesco MARTELLI[1] , Paolo ADAMI[1], Elisabetta BELARDINI[1]

[1] Energetics Department "Sergio Stecco"
University of Florence
Via S Marta,3 –Firenze 50139, ITALY

ABSTRACT

The knowledge of the time resolved flow features can provide a deeper understanding of important aero-thermal effects mainly in transonic annular cascades. A fully 3D and unsteady CFD solver is applied to an HP turbine stage for the investigation of unsteady rotor stator interaction.

The code is a multi-block and parallel solver based on an upwind TVD (Total Variation Diminishing) finite volume scheme. The numerical approach is developed for hybrid unstructured grids. Turbulence is modeled using the classical two equation k-ω model .

A brief description of the cascade, experimental set up and measuring technique is provided. Time accurate CFD computation of pressure fluctuations and heat transfer Nusselt number are compared with the experimental results.

A general good agreement is observed, assessing the validity of the implemented unsteady approach for the description of potential, viscous and shock interaction. Some inaccuracies are revealed by the computed unsteady pressure field. They may be related to the excessively simplified modeling of the coolant injection area or the poor grid refinement in the shock reflection regions. In these areas very strong pressure gradients are experienced by the flow field.

Besides some underestimation of heat transfer rate after the transition onset is detected. This may be reduced through the implementation of advanced turbulence approaches and assessed transition models.

INTRODUCTION

The actual flow field in turbomachinery environment is highly three-dimensional and unsteady. Flow unsteadiness can be related to different concurrent physical mechanisms: potential, viscous and shock effects. Potential flow interaction are associated with the not uniform pitch wise pressure which develops inside each blade vane. This irregular distribution can influence the field on the following rows and is relevant when the axial gaps are small. Viscous phenomena are responsible for the growth of boundary layers and wakes. Their evolution in the downstream row channels causes viscous unsteady interactions. In transonic turbine stages shock systems can detach at the trailing edge and cause shock interactions with adjacent blades and related pressure fluctuations. All these mechanisms require careful investigation for a better understanding and prediction of performance and heat transfer mechanisms in turbine stages.

Flow complexity is further increased by the widespread use of cooling techniques to prevent the overheating of turbine blades. This problem is experienced in the first NGV trailing-edge area and the leading-edge region of the first rotor row. However film cooling devices can be responsible for the generation of a complex unsteady flow pattern in the injection area and influence heat transfer and temperature distribution on the metal. Besides, some apparently local geometrical features of modern gas turbines (such as disk leakage geometry, blade tip gaps, the shape of cooling slots/holes…) have revealed strong potential impact on losses generation and heat transfer mechanisms in the whole blade passage. As a consequence the proper design and analysis of turbine stage details has acquired great relevance.

Considerable amount of numerical and modeling activities has been devoted to the investigation of stator/rotor interaction through the solution of Navier-Stokes equations. Significant results have been obtained with multi-stage steady approaches applying circumferential averages of the fluid dynamic flow features. These methodologies have been successful applied for engineering design purposes mainly thanks to the Adamczyk et all (1990) and Dawes proposals.

First attempts for unsteady stage interaction were reported by Rai using patched grids and approximated stator/rotor count. In this method, called 'reduced count ratio' approach, the stator or rotor blade numbers is modified allowing for simple arithmetic blade ratios like 1:1 or 2:3. The predicted amplitude and frequency in the stator/rotor interaction can be affected by the bias enforced in the physical problem if the adaptation is relevant. A different approach has been suggested by defining a phase-lagged time and space periodicity. The phase-lagged approach uses one single blade passage for each row. The unsteady flow solution is stored over the physical period on the boundaries of the stator and rotor vanes to ensure the actual periodicity between the two rows. Similarly Giles studied the stator/rotor interaction with 1:1 count ratio through a 'time-inclined' marching concept. Differently from the reduced blade count ratio approaches, the phase lagged method and the approach of Giles do not introduce any modification to the actual geometry and a smaller computation domain is required. However large memory storage is involved, while the handling of more than two blade rows interaction is not allowed.

Sometimes the numerical costs and complexity of accurate CFD prediction of unsteady effects and time resolved heat transfer

phenomena in turbo machinery stages are too high for use in routine design. Accordingly simplified loosely coupled approaches have been proposed and investigated by several authors: Hodson Dorney et all (1996) Ho and Lakshminarayna However the modern design requires the unsteady analysis of stage's stator-rotor interaction including 3D effects, hub-shroud-blade heat transfer, cooling and leakage flows. New upgraded CFD techniques have been developed and assessed to provide accurate unsteady predictions to help in the design and engineering procedure. At the same time new advanced computational resources (powerful workstations and mainly parallel architectures) are nowadays available for the handling of this challenging problem within acceptable costs and computational memory and time requirements.

The physical modeling of turbulent and transition phenomena still represent critical aspects for the final assessment of a really general accurate and affordable approach in complex industrial applications. At date the conventional turbulence modeling implemented in CFD solvers for unsteady computations is based on the eddy-viscosity concept and two equation closures approach or in the simplest cases on algebraic modeling. More accurate approaches DNS and LES are impracticable for multistage environments in view of the extremely fine grid resolution required and the related long computing times.

In the present work a reduced count ratio unsteady approach is applied to the aero-thermal analysis of a turbine stages. The effect of both numerical features and physical modeling on the accuracy and performances of the unsteady approach are discussed and compared against the experimental data. The data are extracted from the research activities performed on the VKI stage rig within the framework of the BRITE EURAM project TATEF.

NUMERICAL METHOD

Basic features of the solver

The compressible Navier-Stokes equations are written in the strong conservative form for a perfect gas. The solver is better documented in Belardini et al.. Only a brief description will be given here. The solver is based on an iterative implicit time-marching solution scheme of the discretised differential equations. The implicit iterative time-relaxed Newton method is applied along with the linear solver GMRES coupled to an incomplete ILU(0) factorisation matrix used as preconditioner of the linear system. The spatial discretization is based on an upwind TVD (Total Variation Diminishing) finite volume scheme developed for hybrid unstructured grids. The Roe's approximate method is used for the upwind scheme and a least-squares linear reconstruction of the solution inside the elements provides a second order accuracy. Monotonicity of the solution is ensured through the TVD concept based on a non-linear slope limiter. Significant memory savings and reduction of the overall CPU costs have been obtained by the implementation of a multi-block strategy. The main benefit of the domain decomposition procedure lays in the reduced dimensions of the linear system matrix during the implicit marching of the solution. Further improvements of the performance of the solver have been obtained with the parallel version of the code. Parallelization exploits the division of the domain in smaller blocks which are distributed to the different processors. The standard MPI message passing libraries are used to manage communications between the processors.

An implicit residual smoothing technique enforces the connections of grid regions which are computationally divided by the domain decomposition. In the present application the residual smoothing technique is applied separately to the blocks belonging to the same processor. This choice, maybe providing a penalty in the effectiveness of the residual smoothing procedure, avoids any increase in the communication costs.

Time accurate approach

The time accurate computations of the Navier-Stokes equations can be performed choosing one of the three following options available in the solver: 1) Three steps backward dual time-stepping with implicit Newton-relaxed time marching; 2)Three steps backward dual time stepping with explicit time marching;3) Multi-step explicit time accurate Runge-Kutta method

The dual-time stepping schemes 1) and 2) are based on the addition of a numerical time derivative of the solution vector to the physical unsteady Navier-Stokes equations.

$$\underbrace{-\frac{\partial Q}{\partial \tau}}_{\substack{numerical \\ derivative}} = \underbrace{\overbrace{\frac{\partial Q}{\partial t}}^{\substack{physical\ time \\ derivative}} + \overbrace{\widetilde{R}(Q)}^{spatial\ gradients} - \overbrace{\widetilde{S}(Q)}^{inertial\ terms}}_{unsteady\ equations}$$

The three steps backward formula (second order accurate in time) is used to compute the physical time derivative. The dual-time stepping approaches are used to converge at each physical time level. In the fully explicit Runge-Kutta scheme 3) the following steps provide the time accurate solution of the unsteady Navier-Stokes system:

$$Q^{(0)} = Q^n$$

$$Q^{(k)} = Q^n - \alpha_k \frac{\Delta t}{V}\left[R\left(Q^{(k-1)}\right) - S\left(Q^{(k-1)}\right)\right] \quad k = 1, nk$$

$$Q^{n+1} = Q^{(nk)} \qquad \alpha_k = \left[1/15, \ 7/45, \ 2/7, \ 1/2, \ 1\right]$$

The implicit residual smoothing above mentioned is applied in the internal sub-iterations of dual-time stepping schemes to improve the stability and convergence of the method. In the explicit Runge-Kutta method no special tool is applied to improve stability and robustness.

Physical modelling

Turbulence model is the classical two equation k-ω approach proposed by Wilcox. It is based on the hypothesis of Boussinesq for the computation of the turbulent stresses from the mean field strain. The two transport equations are solved for the turbulent kinetic energy k and its specific dissipation rate ω.

The turbulence model includes an additional algebraic equation which enforces Durbin realizability constraint on the turbulent time scale. This correction helps to reduce the problem of the unbounded growth of turbulent energy in presence of large rates of strain and moderate initial levels of k. This situation is typical at stagnation points ('stagnation point anomaly'), in the boundary layer development and large strain areas occurring in the middle of a

turbine passage. The realizability constraint is enforced on the turbulence time scale T as follows:

$$T = \min\left\{\frac{1}{C_\mu \omega}, \frac{1}{C_\mu \sqrt{6S}}\right\} \text{ with } S = \sqrt{\frac{1}{2}\left(\frac{\partial u_i}{\partial u_j} + \frac{\partial u_j}{\partial u_i}\right)^2}$$

T equals k/ε in the $k-\varepsilon$ model and $1/(C_\mu \omega)$ in $k-\omega$ model. For compressible flows S should be replaced by $S^* = S - 1/3*(\nabla U)$.

For the present 3D multiple row simulation 1-3 millions grid elements are required in view of the very fine grid resolution required by specific areas. Very refined meshing and severe grid clustering is necessary for instance on the rotor surface which is directly affected by film cooling ejection and where the heat transfer rate is relevant. To reduce the global number of nodes a more relaxed clustering is applied near adiabatic walls. The drawback of this technique is that in the coarser regions the grid spacing in the low-Reynolds number viscous layers may not be sufficient for the consistent application of the turbulence transport equations. To overcome this limitation the wall function approach has been introduced. The wall function approach is based on the assumption of constant shear stress and local equilibrium of turbulent kinetic energy. If applied for the aero dynamical prediction of attached flows, the use of wall functions provides a simplified approach for the computation of the viscous stresses, turbulent kinetic energy k and specific dissipation rate. These functions can be used to bridge over the first grid point and the solid wall and can replace the exact solution of the transport equation for the turbulent variables. The modified expressions proposed by Huang and Zhu (1997) has been implemented in the solver in view of their capability to include compressibility effects in the laws of the wall. The applied relationship are:

$$U_c^+ = \frac{U_c}{U_\tau} = \frac{1}{k}\ln(Ey^+), \; k=0.41, \; E=8.4317$$

$$U_c = \sqrt{B}\left[\sin^{-1}\left(\frac{A+U}{D}\right) - \sin^{-1}\left(\frac{A}{D}\right)\right],$$

$$A = (q/\tau)_{wall}, \; B = \frac{2T_{wall}}{(\gamma - 1)P_{rt}}, \; U_\tau = \sqrt{(\tau/\rho)_{wall}}$$

$$D = \sqrt{A^2 + B^2}, \; y^+ = \mathrm{Re}\, U_\tau y(\rho/\mu)_{wall}, \; k = \frac{(\tau_{wall}/\rho)^{3/2}}{0.3},$$

$$\omega = 0.3\frac{(\tau_{wall}/\rho)}{ky}$$

In the solver the detection of the local y^+ value during the numerical computation allows the automatic coupling of the wall functions with the two equations turbulence model. In fact the solid boundary conditions are imposed using the wall functions only when the nearest grid cell is located at a non dimensional distance $y^+ > 11$. Otherwise the standard low Reynolds approach is followed. This way the selection of the more suited boundary condition is guaranteed. At the same time a flexible node distribution around the solid boundaries is allowed during the grid generation process according to the different accuracy requirements of different portions of the physical domain.

EXPERIMENTAL SETUP

VKI HP stage description

The stator row consists of 43 untwisted cylindrical vanes, while the rotor row consists of 64 twisted blades (Figure 1-b). Coolant ejection is realized through a slot along the NGV rear pressure side (Figure 2). In this transonic HP turbine stage, potential, viscous and shock interaction flow unsteadiness are present, although the shock wave interaction is the dominant mechanism. The role of unsteadiness is relevant in this stage in view of the high ratio between the period of the fluctuating disturbance (mainly the stator TE shock) and the time required by a fluid particle to travel through the rotor.

Test facility and measurements techniques

The stage has been tested in the CT3 short duration compression tube facility (an isentropic light piston wind tunnel) at VKI. In this facility Reynolds and Mach numbers, gas/wall and gas/coolant temperature ratios can be adjusted in ranges representative of modern high pressure turbines. Constant flow conditions can be maintained for periods ranging between 0.1-0.4s. The wind tunnel design (a blow-down type facility) is reported in Figure 2-a. The operative principles for annular cascade testing are accurately described by Sieverding and Arts

The time averaged pressure profile near the hub and tip end-wall and exit plane is obtained by means of Kulite transducers; the estimated accuracy of the measurements is about +/- 20 mbar. The averaged downstream flow angle and total pressure are also measured by means of a five hole probe and.

1-a) Stage Configuration   1-b) The twisted rotor
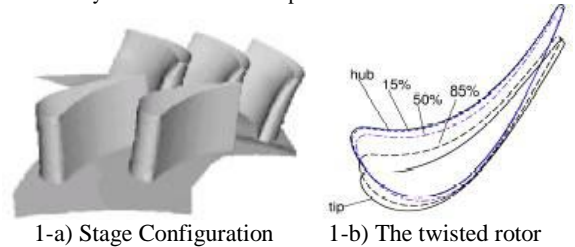
	Stator Row	Rotor Row
Axial Chord	43.057 mm	39.59 mm
Pitch	8.372°	5.625°
Mean Radius (inlet)	369.85 mm	369.7 mm
Mean Radius (outlet)	369.85 mm	367.3 mm
Blade Height (inlet)	50.7 mm	50.7 mm
Blade Height (outlet)	50.7 mm	55.8 mm
Blade Number	43	64
Rotat. Speed (RPM)	0.	6500

1-c) Stage geometric characteristics

Figure 1– Geometry and Characteristics of the Stage

The rotor blades were instrumented with 24 fast response piezo-resistive semi-conductor sensors at three the different radial sections (15%, 50% and 85% span). In Figure 7 the gauge positions for mid span height are shown. Unsteady pressure fluctuations are available for the comparison with CFD results. The fast response sensors for time resolved fluctuations are placed in cylindrical

housings in the casing and connected to the surface of the end-wall by a 0.2mm long duct with a diameter of 0.8mm diameter. (Dénos and Sieverding (1997)). The chips have natural frequencies up to 400 kHz.

The time averaged temperature distribution for turbine stage inlet and outlet have been obtained with classical K type thermocouples. The unsteady wall temperature on the rotor is measured with film gauges consisting of a thin metallic strip laying on a ceramic insert. The heat transfer rate used in the Nu number definition is computed from the integral of temperature history. For further details about the testing features and experimental activities the work of Dénos should be considered.

Test conditions

Various measurement campaigns are available with a fixed cooling mass flow rate of 3% and nominal rotor speed (6500 RPM). The present CFD application focuses on the nominal unsteady flow field conditions: reference Reynolds Number ($\approx 10^6$), nominal total temperature $T_{01} = 439K$ and nominal pressure ratio $(p_{01}/p_2) = 3.04$. For this working condition the mid-span isentropic Mach number at the NGV exit is 1.08 while at the rotor exit is 0.42 in the absolute frame. The flow field experiences a transonic regime both in the stator and the rotor blade (outlet relative mach number about 0.89). For unsteady heat transfer computations a constant blade temperature has been applied, equal to 295K with a coolant total temperature of 439K.

DISCUSSION OF RESULTS

Stage Modeling

For this stage configuration the blade count ratio of the two rows is very close to 2:3 (0.6718 against 0.6667). Accordingly the reduced count ratio approach has been applied and the stage geometry has been slightly modified. The exact 2:3 periodicity has been obtained with a scaling of 0.7%. The scale reduction factor has been applied to the rotor vane only because the NGV is chocked.

Previous unsteady viscous/inviscid computation have demonstrated that the main frequencies and the unsteady behavior of the system are not remarkably affected by this approximation. The NS equations are solved in a rotating reference frame for the rotor blades. As a consequence a body fitted mesh can be generated for all the moving parts and tip leakage (Figure 3-b). The grid generation process has been carried out to ensure high accuracy of the final time resolved simulation. For this reason a very realistic modeling of the stage geometrical features has been performed in the refined GRID 3. The detailed representation of NGV coolant ejection slots (Figure 2-a) and the rotor tip leakage clearance (Figure 3-b) has been performed.

The matching of the stator and rotor rows is pursued through a sliding plane approach developed for general unstructured grids (Belardini et all).

Grid Sequencing

The high computational costs involved in this demanding computation can be reduced exploiting different effective acceleration techniques available in the solver. A faster convergence of the solution can be obtained through the implicit time-marching, the block-diagonal ILU preconditioning, the local time stepping and the residual smoothing approach. A more noteworthy reduction of the global computing time has been accomplished by the 'grid sequencing strategy'.
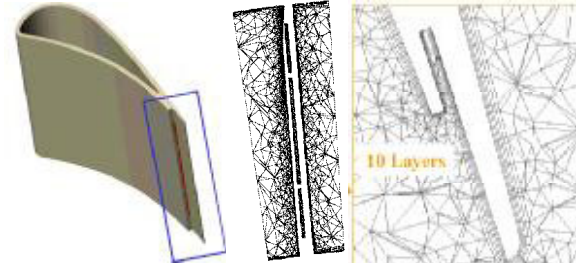
Figure 2 NGV blade with TE coolant ejection
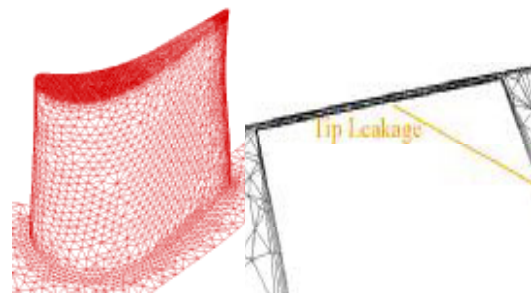
Figure 3-Rotor blade with tip leakage

This technique is based on the use of a family of grids with increasing refinement for both spatial accuracy and time resolution. The coarser grids are faster and efficient to reduce the disturbance induced by an erroneous initial guessed solution, but the converged solution can neglect some important flow features. Nevertheless the raw flow field obtained with the coarse grid can be profitably used as a starting point for more accurate simulations. Improved time and space solutions can be obtained in fewer passages on the refined grids starting with an almost exact solution. A general 3D linear interpolation routine consistent with unstructured grids has been developed to transfer the solution between grids with a different number of elements.

GRID	N.lements	Accuracy allowed	Time teps
1	600000	Potential and shock interaction	100-500
1	700000	Averaged pressure profiles	100
2	1.8E6	Wake interactions	200
3	4.0E6	Heat transfer fluctuations	500

Table 1: Grids sequencing

In the present computation the grid sequencing technique has been applied using four grids; the basic features of each grid are listed in Table 1. Some details about the grid used for final HT computations are plotted in figure 4. The first initial solution field has been obtained using two different grids (GRID 1 in table1) with almost

the same number of elements and about the same computational cost: the first in the inviscid approximation, the second in the laminar assumption. On these coarser grids the development of the basic features of the unsteady aerodynamic field could be successfully accomplished with a quite fast removal of the flow initialization error. The average residual, the mass fluctuations and the periodicity of the rotor pressure fluctuations have been used to assess the required convergence level at each grid step. The viscous and inviscid numerical solutions on the coarse grids showed some differences. This is due to the grid sensitivity typical of the coarse grids in which the solution can be dependent on the location of nodes inside computational domain. The mesh is clearly different in the coarse grids in the viscous and unviscid assumption. In fact a relevant number of elements can be placed in the main core of the flow for the inviscid case. Instead for the viscous computation the clustering of several elements is required along solid boundaries and inside the prismatic layers. The converged solution is affected by this different element distribution. Despite these differences in the intermediate flow field, the final converged solution obtained on GRID 2 and GRID 3 is the same. Both the coarse computations could be completed on a cluster of four DEC ALPHA-XP1000-666 Mhz workstations. The final HT computation has been carried out with 5 hundred subdivisions of the periodic angular pitch (2 NGV:3 rotor). For the nominal rotational speed of 6500 RPM the corresponding numerical sampling frequency was of about 1MHz. In a preliminary phase the unsteady HT computations have been performed both with the explicit and implicit dual-time stepping scheme. The performance of the two approaches which can be used to drive the convergence of the solution at each physical time step have been compared. The results showed that, for a fixed residuals reduction, the explicit scheme required about 60 iterations for the convergence of the instantaneous flow field. For the implicit time marching 10 numerical sub-iterations were sufficient. Therefore the overall CPU time required by the explicit dual-time stepping approach was higher (further discussion is not reported here for conciseness). For this reason the unsteady HT run was completed using the implicit dual time stepping approach.
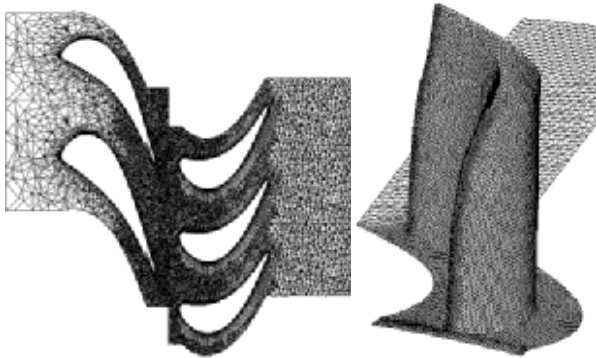
Figure 4: 3D stage computation (final GRID 3)

The final time accurate computation run on a Beowolf Linux cluster of 16 PIII 1.3GHz.

Time averaged comparisons

The time-averaged static pressure profiles on the rotor blade are reported in the Figure 5 and plotted against curvilinear abscissa.

A slight under prediction of flow acceleration on the suction side is present in the lower portion of the blade and the mid-plane.

Steady single blade computations have been performed showing that this could be caused by a slight underestimation of the local rotor incidence that is felt from hub until the blade midspan. A possible explanation for this incidence defect could be represented by the presence of hub-disk leakage in the real stage, which is not reproduced in the computations. Despite this, the agreement with experiments in all the three radial section is globally acceptable and especially near the tip region the pressure distribution of the experimental result is quite well reproduced by computed time averaged profiles. Downstream the blade suction side crown the agreement improves also at 15 and 50% of the span and the expected recompression shocks is well captured

Averaged rotor pressure - 85% span   Averaged pressure – 15% span

Averaged pressure 50% span
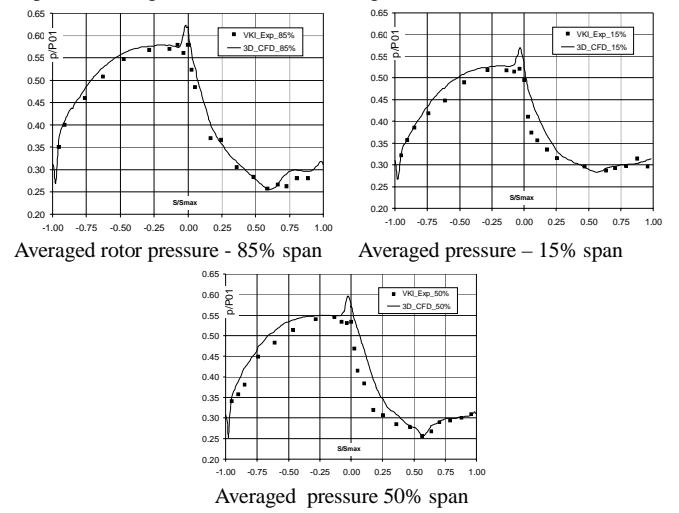
Figure 5: Time averaged Pressure Profiles

For heat transfer computation Nusselt number is computed according to the following classical definition:

$$Nu = \frac{qc}{K_{gas} \cdot (T_{gas} - T_{wall})} = \frac{hc}{K_{gas}}$$

Here c is the blade chord and K_{gas} the thermal conductivity of the gas, q is the wall heat flux. T_{wall} and T_{gas} are the wall and the mean total relative temperature of the gas respectively. The blade temperature is assumed constant and equal to the environment temperature (295K) while T_{gas} is computed from ratio $T_{gas}/T_{walls} = 1.5$ reported in figure 2-c. The inlet turbulent viscosity level is 5%.

In figure 6a the experimental and computed time averaged Nusselt values are compared. The isentropic mach number distribution is reported in Figure 6b. Some physical considerations about the features and development of the boundary layer may provide suggestions to understand the basic heat transfer physics in the rotor blade. In the first half of SS till around 60% of the blade, the increase of the M_{is} indicates a continuous acceleration of the flow, which, starting from rest at LE, reaches transonic conditions. The favorable pressure gradient exerts a stabilizing effect on the growing boundary layer which presumably retains a laminar regime. Around 60% of the blade SS the isentropic mach number in Figure 6b decreases, indicating an abrupt flow deceleration maybe

promoting transition to the turbulent state. In the final portion of the SS the isentropic mach number is almost constant. On the PS the isentropic Mach number distribution is progressively increasing from the LE to the TE.

a) Nusselt Averaged Results

b) Mis averaged Results
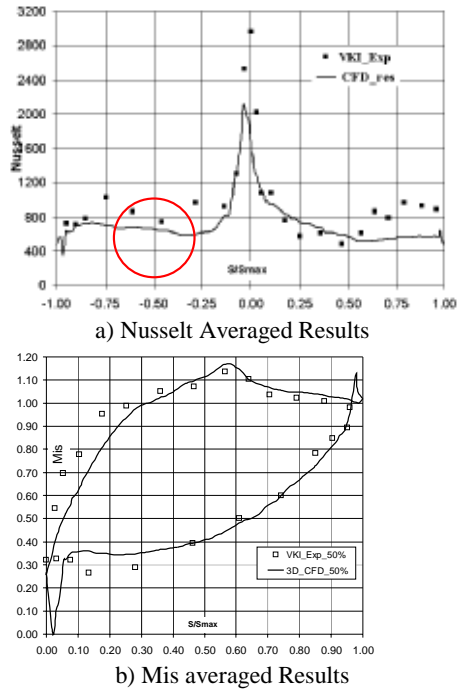
Figure 6: Time averaged Results – Pressure and Nusselt

At the blade leading edge the numerical heat transfer seems to follow the experimental distribution: the typical experimental Nusselt peak in the LE region, associated with the absence of insulation effects of the boundary layer in the stagnation area, is reproduced by the numerical results. This is probably allowed by the good grid quality in this region and by the laminar nature of the boundary layer developing on the LE of the blade. With the laminar boundary layer development on both suction and pressure sides the Nusselt number decreases rapidly due to the thickenings of the boundary layer. As expected, in this early front region of the blade, the boundary layer is thin. The heat transfer rate depends mainly on the potential blades interaction and on the free stream turbulence intensity. The unsteady pressure fluctuation obtained by numerical computations, in this leading edge region of the rotor blade are in good agreement with experimental results and thus also the Nusselt number prediction perform quite well.

Downstream the nose of the blade (after 50% of the abscissa) on the suction side, the heat transfer rate is somewhat under predicted. Looking at the experimental data it is possible to argue that in this region the boundary layer may undergo a fully turbulent transition. The transition is presumably triggered by the interaction with the shock detaching from the NGV TE. The reduced agreement between experimental and numerical heat transfer levels is in the last portion of the blade can be attributed to the limitations of the turbulence closure implementation. In fact the classical two equation k-ω approaches usually fail for the detection of the transition onset. At date no specific transition correction is embodied.

On the PS around the blade LE, the surface boundary layer develops on a convex surface, and a region of rapidly accelerating flow is encountered. The increase of velocity causes the strong decrease of Nusselt number in the first 10% of the blade. In the concave portion of the central PS the boundary layer thickness is globally increasing due to the favorable stream wise pressure gradient. The strong curvature of the blade surface has a destabilizing effect and provokes an increase of the turbulence level in the boundary layer, depending both on the blade curvature and the free stream turbulence level. Also in this case the linear k-ω closure is expected to fail in predicting the curvature effect onto turbulent production. The Nusselt number initially grows when strong convex curvature is encountered while it decreases toward the central parts of the PS following the increase of the boundary layer. Finally in the last part of the PS the boundary layer is accelerated. The isentropic Mach number stabilizes and boundary layer thickens leading to a decrease of the Nusselt number. The capability of the averaged numerical results to follow these effects is less clear on the PS side with respect to the SS side. As mentioned the reduced agreement between experimental and numerical results has to be attributed to the turbulence development inside the boundary layer and its interaction with the concave curvature of the wall surface.

Unsteady pressure fluctuations

In the present paragraph the computed unsteady aero thermal flow field is discussed against the experimental results. Figure 7 shows pressure fluctuations $\Delta p/P01 = \left(p - p_{averaged}\right)/P01$ for different rotor blade locations at mid-span. The selected points lay on the suction and pressure side at approximately 20% axial chord (point 4 and 16 respectively), on the leading edge (point 14), on suction and pressure side near the TE (point 12 and 22). On the abscissa the phase spans from 0 to 2 when a complete periodic passage is completed (e.g. 2 NGV vanes and 3 rotor blades). From experimental data it is evident that pressure fluctuations can be perceived all over the rotor blade. They can be related to the passage of the vane TE fish tale shock. Besides, due to the relative movement of the rows, the position of the shock is not fixed but periodically oscillates around the axial direction from about +20° to –20°.In the experiments the maximum pressure fluctuations can be detected in the area of strong curvature in the LE of the rotor suction side due to local lower pressure levels. The high amplitude of the unsteady fluctuations is clearly indicated by the pressure traces on gauge 4 of Figure 7. The basic features of the instantaneous signal are reproduced by the numerical results, even if peak values are slightly under predicted. This behavior seems coherent with the aforementioned incidence defect between numerical and experimental results. The underestimation of the incidence angle could explain both the reduction of pressure peaks and their different phase location (see the averaged pressure profiles of Figures 5 and 6). Besides near gauge 4 location the stator wake hits the rotor blade almost tangentially. This could provoke a complex interaction between the developing rotor boundary layer and the stator wake. Close to phase 0.7 a small pressure plateau is perceived in the experimental data. It appears only a bit more pronounced in the computational results. However, the effect played on the local predicted heat transfer rate is significant, as will

be better underlined in the next section.

The shock hitting the rotor decreases its strength towards the stagnation point (gauge 14) of the rotor blade where static pressure reaches the relative inlet total value. The kink in the pressure profile visible at a phase angle of approximately 0.5 should be related to the interference of the stator wake with the rotor blade. The agreement between experimental and numerical results is acceptable: the maximum peak value behaves consistently with the estimate observed for the averaged pressure values of Figure 5. On the pressure side two peaks close to the leading edge can be detected: one is supposed to be due to the direct impinging of the wake while the other to the reflected shock coming from the leading edge of the proceeding blade (see Figure 8). The intensity of this reflection is not well reproduced although the effect is present in the numerical results (Gauge 16). This could indicate a poor grid refinement in this specific area or most likely an insufficient time resolution. The error is less pronounced in the rear portion of the blade (gauge 22) where the agreement with the experiments proves to be better. The effect of the under prediction of wake reflection is also appreciated from the M_{is} averaged profile evidenced in Figure 6.b for s/smax=0.2. The same effect is expected to explain the Nu rise in experiments and not in computation centered on the same location in figure 6.a.
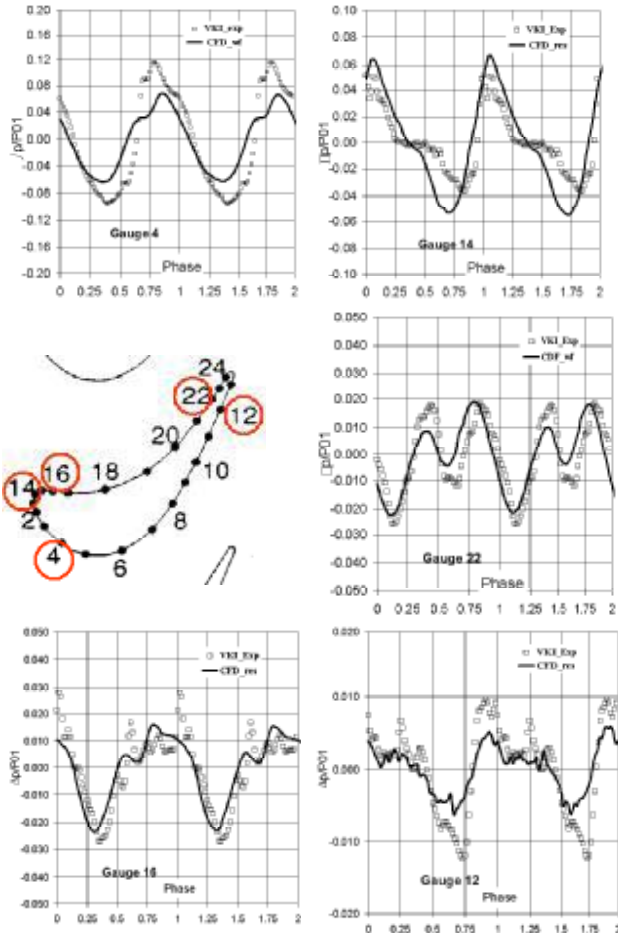
Figure 7 – Unsteady pressure fluctuations

In the final part of the suction side (gauge 12) the shock fluctuations are not felt, while the wake coming from the TE the stator has almost completely mixed with the downstream uniform flow. For these reasons the amplitude of unsteady fluctuations is one order less intense. Besides the boundary layer is thicker because of the decreasing Mach distribution (Figure 6) and the turbulent unsteady fluctuations become relevant (in fact several peaks can be detected). The accuracy of the numerical result is quite good despite the transitional nature of the boundary layers while the amplitude of the peaks is slightly underestimated.

Unsteady turbulent viscosity and heat transfer rate

In Figure 8 the instantaneous turbulent viscosity and pressure contours at 50% span are reported for two different relative positions. The NGV TE wakes can be clearly identified by the high turbulent regions impinging on the rotor LE. These plots confirm that turbulence production in the NGV is essentially caused by the SS boundary layer. Its growth is located mainly in the adverse pressure gradient of the last part of the blade. No appreciable stall is observed on the NGV and the boundary layer detaches in correspondence of the stator TE region, diffuses and finally impinges on the rotor blade. On the pressure side the boundary layer is thinner, due to favorable pressure gradient experienced by the flow field in most of wall surface. On this side of the blade the most of turbulent viscosity is introduced by blade cut housing the coolant ejection. The shape of the wake from the NGV is almost independent from the relative position between the two rows.

a) phase location=0.75

b) phase location=1.25
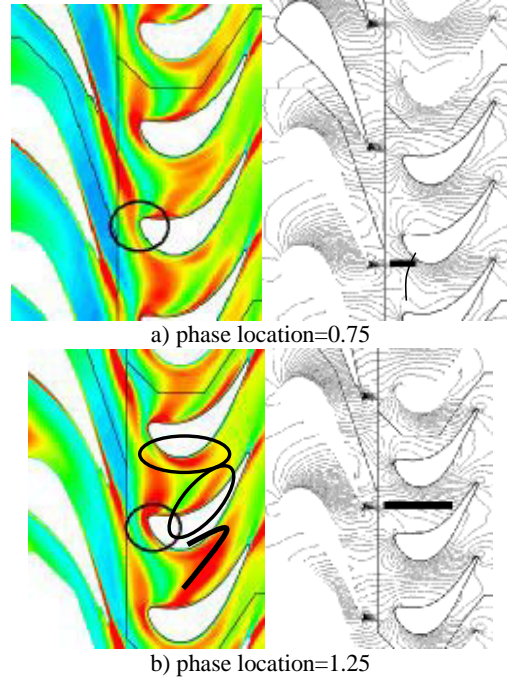
Figure 8: Istantaneous Viscosity Contours

When the wake moves toward the rotor blade the effect on the flow can be different depending on the relative position of the two rows. For some positions the wake impinges directly on the LE of the blade and is split in two different branches, the first traveling on the PS and the second on the SS. After a half period the wake impinges directly on the blade PS. A high turbulence bubble develops and

grows. The flow in the vane convects the turbulence bubble downstream with a not uniform rate and a clear stretch of the wake is observed from the pressure side to the suction side. Apparently due to this action the wake turbulent bubble breaks into two branches.

The shape of the unsteady pressure signal can be endorsed mainly to potential interactions and shock reflection mechanisms. The viscous interaction and wake passages can be perceived only as small plateaus in the time resolved pressure fluctuations. For the unsteady heat transfer prediction also the wake interaction and the turbulence viscosity level become relevant because they can influence the level of the heat transfer. From the experimental time resolved Nusselt number the shock impingement in the leading edge region seems to be the main cause of the large Nusselt number fluctuations.
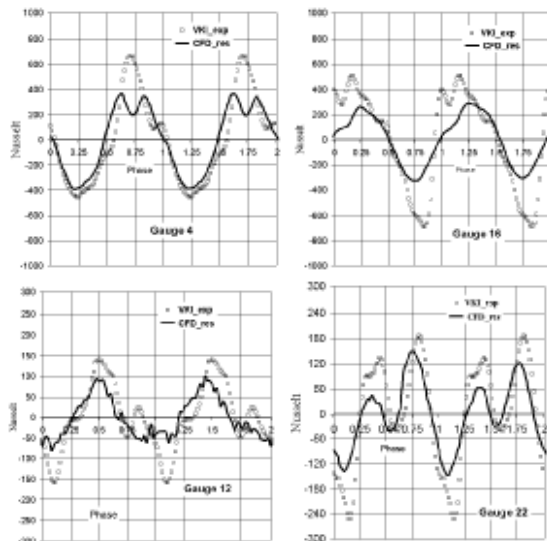
Figure 9: Nusselt Number fluctuations

In figure 9 the unsteady heat transfer rate is plotted for different positions on the rotor blade. The amplitude of Nusselt number fluctuations varies depending on the measurement location following the same trend of the pressure signal. The highest amplitude are seen in the crown (gauges 3 and 4). In gauge 4 the minimum value (–400 units) of heat transfer is detected in the situation shown in figure 8b when the rotor surface is not directly hit by the stator wake. The maximum level of the Nusselt number (+600) is obtained when the shock is located exactly in the gauge area and the wake impinges on the PS of the neighboring rotor blade as shown in figure 8a. The numerical results show a double kink not revealed with the same intensity by the experimental results. This is presently not well understood although it seems to be connected with the plateau observed in pressure profile of Figure 7. This local effect may be generated by the modeling of the coolant ejection from the blade NGV TE with respect to the real configuration. Therefore it is argued that a spurious expansion fan not merging with the shock system is somehow generated at the NGV cut and travels downstream with a reflection on the neighboring NGV blade before impinging onto the rotor LE. Accordingly, a new minimum in heat transfer is supposed to be added thanks to the magnification of this effect in the prediction of

gauge 4 in Figure 9. Nusselt number fluctuations on gauge 16 on the PS show an opposite trend with respect to gauge 4 on the SS and the amplitude of Nusselt number fluctuation are slightly reduced. In the experimental results a double peak appears, caused both by a direct shock impingement, preceded by a smaller one due to a shock reflection coming from the leading edge of the adjacent blade which slightly underlined in the numerical as already noticed: Differently from pressure profiles in the same gauge, the agreement is better probably because wake and viscous effects need also to be considered for the heat transfer rate. The same conclusions may be applied to the central part of the blade pressure side as can be shown also in gauge 22.

CONCLUSIONS

The unsteady computation for stator/rotor interaction has been presented considering 3D viscous conditions in a transonic cooled turbine stage. The numerical tool is based on a Navier-Stokes solver consistent with unstructured grids and different time accurate schemes of second order accuracy. A 2:3 vanes exact periodicity has been used owing to the almost exact blade count ratio of 43:64 blades in the actual rig. The application reports the results achieved in terms of time averaged and time resolved pressure and heat transfer data on the rotor blade.

The results allowed satisfactory prediction of shock and potential interaction with a quite demanding discretisation of the flow domain and accuracy of time resolution. The potential interaction and shock interaction are actually playing the major role also in the stage interaction also for unsteady heat transfer prediction. Viscous wakes and the turbulence development inside and outside the boundary layers proved to be of great relevance mainly for the unsteady pressure and heat transfer behavior especially moving towards the blade trailing edge. This viscous interaction appeared to be resolved with some minor inaccuracies revealed both by the pressure and heat transfer comparison. The better prediction of these viscous unsteady features for pressure and heat transfer maybe could be accomplished with some improvement of the turbulent modeling, such as the implementation of a transition correlation to the present turbulence closure.

Acknowledgments

References

Adamczyk, J.J., Celestina, M.L., Beach, T.A. and Barnett, M. "Simulation of 3D Viscous Flow within a Multistage Turbine" J. of Turbomachinery, Vol. 112, 1990.

Adami, P. Belardini E., Martelli F., 'Unsteady Rotor/Stator Interaction: An Improved Unstructured Approach' 2001-GT-0356, ASME TURBO EXPO 2001, USA June 4-7, 2001

Adami P., Michelassi, V., Martelli F., (1998), Performances of a Newton-Krylov scheme against implicit and multi-grid solvers for inviscid flows , AIAA paper 98-2429.

Belardini E., Adami P., Martelli F. *"Development of an Unsteady Parallel Approach for 3D Stator-Rotor Interaction"* 4th

European Conference on Turbomachinery, Fluid Dynamics and Thermodynamics- Firenze 20-23 March 2001

Dawes, W.N., "Toward Improved Through-Flow Capability: the Use of 3D Viscous Flow Solvers in a Multistage Environment" J. of Turbomachinery, Vol. 114, Jan 1992.

Dénos R., Sieverding C.H., (1997):"Assessment of the Cold Wire Resistance Thermometer for High Speed Turbomachinery Application". Transactions of ASME. *Journal of Turbomachinery*. January, Vol. 119, No. 1, pp. 140-148.

Dénos R., Sieverding C.H., Arts T., Brouckaert J.F. and Paniagua G., 1999, "Experimental Investigation of the Unsteady Rotor Aerodynamics of a Transonic Turbine Stage", 3rd European Conference on Turbomachinery. London.

Denton J., D., "The Calculation of Three-Dimensional Viscous Flow in Though Multistage Turbomachines" J. of Turbomachinery, Vol. 114, Jan. 1992

Dorney, D.J., Davis, R.L. and Sharma,O.P. "Unsteady Multistage Analysis Using a Loosely Couple Blade Row Approach" J. of Propulsion and Power, Vol. 12, No2, 1996.

Durbin, P.A., "On the k-e Stagnation Point Anomaly", Int. J. Heat and Fluid Flow, 1996, 17.

Erdos, J. I., Alzner, E. and McNally, W., "Numerical Solution of Periodic Transonic Flow Through a Fan Stage", AIAA J., Vol. 15, No. 11, 1977

Giles, M. and Haimes, R. (1993) "Validation of a Numerical method for Unsteady Flow Calculations", Asme J. of Turbomachinery, Vol. 115.

Hah, C. "Navier-Stokes Analysis of 3D Un steady Flows Inside Turbine Stages", AIAA paper 92-3211, July 1992.

Ho, Y.H., Lakshminarayana, B. "A Loosely Coupled Unsteady Simulation of a Single Stage Compressor" IJCFD, Vol 10, 1998

Hodson, H.P. "An inviscid Blade-toBlade Prediction of Wake-Generated Unsteady Flow", J. of Gas Turbine and Power, Vol. 107, 1985.

Huang,P.G. and Coakley T.J. (1993) "Calculation of supersonic and hypersonic Flow Using Compressible Wall Function", 2nd Int. Symp. on Turbulence and Measurements.

Medic,G, Durbin, P.A. (2002) "Toward Improved Prediction of Heat Transfer on Turbine Blade",Journal of Turbomachinery, 2002, Vol. 124 pp 187-191

Rai, M.M., "Unsteady 3D Navier-Stokes Simulation of Turbine Rotor-Stator Interaction", AIAA 87-2058,1987.

Zhu, J. and Shih, T.H., (1997) " CMOTT Turbulence Model for NPARC" NASA CR 204143

Sieverding C. H. and Arts T., (1992): "The VKI Compression Tube Annular Cascade Facility CT3". *ASME Paper* 92-GT-336.

Wilcox, D.C., "Reassessment of the Scale-Determining Equation for Advanced Turbulence Models", AIAA Journal, 1988, Vol. 26, No.11, pp. 1299-1310.